

# Chapter I.1

## History and Principles of Hybrid Imaging

James A. Patton

### Introduction

Positron emission tomography (PET) and single photon emission computed tomography (SPECT) systems are used to image distribution of radiopharmaceuticals in order to provide physicians with physiological information for diagnostic and therapeutic purposes. However, these images often lack sufficient anatomical detail, a fact that has triggered the development of a new technology termed hybrid imaging. Hybrid imaging is a term that is now being used to describe the combination of x-ray computed tomography (CT) systems with nuclear medicine imaging devices (PET and SPECT systems) in order to provide the technology for acquiring images of anatomy and function in a registered format during a single imaging session with the patient positioned on a common imaging table. There are two primary advantages to this technology. First, the x-ray transmission images acquired with CT can be used to perform attenuation correction of the PET and SPECT emission data. In addition, the CT anatomical images can be fused with the PET and SPECT functional images to provide precise anatomical localization of regions of questionable uptake of radiopharmaceuticals. This chapter will provide a review of SPECT, PET, and CT instrumentation and then discuss the technology involved in combining these systems to provide the capabilities for hybrid imaging.

### Single Photon Emission Computed Tomography

For many years, nuclear medicine procedures have been performed using a scintillation camera. Originally, multiple planar projections were acquired to provide diagnostic information, but, more recently, the techniques of SPECT have been utilized. During this time, the scintillation camera has evolved to a high-quality imaging device, and much of this evolution is due to the integration of digital technology into every aspect of the data acquisition, processing, and display processes.

Conventional planar images generally suffered from poor contrast due to the presence of overlying and underlying activity that interferes with imaging of the region of interest. This is caused by the superposition of depth information into single data points collected from

---

J.A. Patton (✉)

Department of Radiology and Radiological Sciences, Vanderbilt University Medical Center,  
Nashville, TN, USA  
e-mail: jim.patton@vanderbilt.edu

perpendicular or angled lines of travel of photons from the distribution being studied into the holes of the parallel hole collimator fitted to the scintillation camera. The resulting planar image is low in contrast due to the effect of the superposition of depth information. This effect can be reduced by collecting images from multiple positions around the distribution and producing an image of a transverse slice through the distribution. The resulting tomographic image is of higher contrast than the planar image due to the elimination of contributions of activity above and below the region of interest. This is the goal of SPECT, i.e., to provide images of slices of radionuclide distributions with image contrast that is higher than that provided by conventional techniques.

## ***Data Acquisition***

### **Instrumentation**

The introduction of the scintillation camera by Anger and Rosenthal in 1959<sup>1</sup> and its ultimate evolution into the imaging system of choice for routine nuclear medicine imaging applications resulted in a great deal of effort being expended toward the extension of the scintillation camera as a tomographic imaging device. In the early 1960s, Kuhl and Edwards established the fundamentals for SPECT using multi-detector scanning systems to acquire cross-sectional images of radionuclide distributions.<sup>2-4</sup> In the 1970s, Muehllehner,<sup>5</sup> Keyes and colleagues<sup>6</sup> and Jaszczak and colleagues<sup>7</sup> adapted this technology to a rotating scintillation camera. The result of these efforts along with the integration of computer systems was the development of the modern day SPECT system as a scintillation camera/computer system with one, two, or three heads and tomographic imaging capability. The scintillation camera collects tomographic data by rotating around the region of interest and acquiring multiple planar projection images during its rotation. It is imperative that the region of interest is included in every projection image. If this is not the case, the resulting truncation of the images will produce artifacts in the final reconstructed images. The camera may move in a continuous motion during acquisition but typically remains stationary during the acquisition of each projection image before advancing to the next position in a "step and shoot" mode of operation. A complete 360° rotation of a scintillation camera with a rectangular field of view will completely sample a cylindrical region of interest. Originally, camera systems were only capable of circular orbits; however, modern day systems have elliptical orbit capability. This is accomplished by equipping the collimators with sensors that detect the presence of the patient and maintain the camera head(s) in close proximity to the patient as the orbit is completed. Since the spatial resolution of collimators used with the scintillation camera degrades with distance from the collimator face, the optimum resolution is obtained in each projection image when the camera is as close to the patient as possible.

Initial SPECT applications were performed with a single-head scintillation camera acquiring data from a 360° orbit as shown in Fig. I.1.1A. When interest in imaging the myocardium became prominent, experimental work demonstrated that acceptable images could be obtained using a 180° orbit (right anterior oblique to left posterior oblique).<sup>8,9</sup> Although this results in an incomplete sampling of the region of interest, this lies in the near field of view of the camera throughout the partial orbit where the spatial resolution is optimum, and images of acceptable quality are obtained. Early in the evolution of SPECT imaging, it became evident that optimum counting statistics for many applications could not be obtained

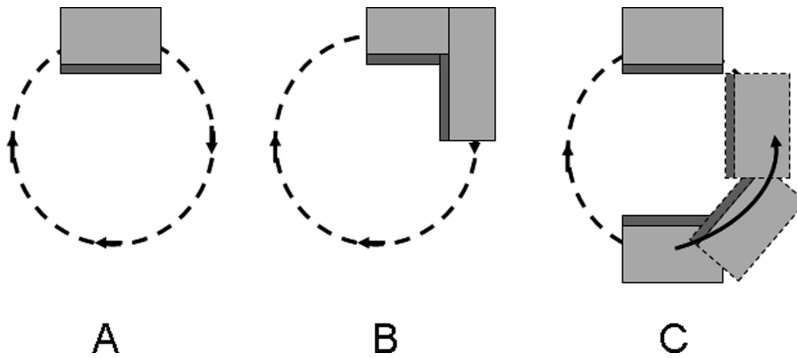


**Fig. I.1.1** Scintillation cameras for nuclear medicine applications have evolved from single-head (A) to dual-head, fixed  $90^\circ$  geometry (B), and finally to dual-head, variable-angle multipurpose cameras (C) (Reprinted with permission of Springer Science + Business Media from Vitola J, Delbeke D, eds. *Nuclear Cardiology and Correlative Imaging: A Teaching File*. New York: Springer-Verlag, 2004.)

in a reasonable time frame that could be tolerated by patients. This situation was remedied by the development of multi-head scintillation cameras. The first system to evolve was a dual-head camera in a fixed  $180^\circ$  geometry permitting a  $360^\circ$  acquisition with only a  $180^\circ$  rotation of the gantry. This development provided a twofold increase in sensitivity for SPECT applications. However, this increase in sensitivity was not available for cardiac applications using  $180^\circ$  acquisitions. To address this problem, special purpose, dual-head cameras were developed with the camera heads fixed in a  $90^\circ$  geometry as shown in Fig. I.1.1B. This made the twofold increase in sensitivity also available for cardiac imaging, and the acquisition of projections through  $180^\circ$  could be acquired with a  $90^\circ$  rotation of the dual-head gantry. Since many scintillation cameras must serve multiple purposes in nuclear medicine departments, the next step was the development of dual-head, variable-angle scintillation cameras as shown in Fig. I.1.1C. These cameras can acquire images with the heads in a  $180^\circ$  geometry for routine  $360^\circ$  applications, and one head can be moved into a  $90^\circ$  geometry with the other head for  $180^\circ$  cardiac applications. The two latter configurations are presently considered the cameras of choice for cardiac imaging.

## Acquisition Parameters

### Collimation

SPECT applications typically make use of parallel hole collimators in order to establish an orthogonal detection geometry with the crystal detectors. Imaging of low-energy radionuclides is generally limited to the use of general purpose, parallel hole collimators.

The resulting images typically exhibited poor spatial resolution. The emergence of multi-head cameras and the resulting increase in sensitivity have made it possible to improve spatial resolution by the use of high-resolution collimators, and these collimators are now the choice for most imaging applications.

### Matrix Size

For most SPECT applications, the acquisition matrix size for acquiring planar projection images is typically a  $64 \times 64$  data point array. The decision is based on the size of the

smallest object to be imaged in the distribution being studied. Sampling theory states that in order to resolve frequencies (objects) up to a maximum frequency (smallest object) at least two measurements must be made across one cycle (the object). This maximum frequency is referred to as the Nyquist frequency. For example, using a camera with a 540-mm field of view, a zoom factor of 1.4 and a  $64 \times 64$  acquisition matrix size would result in a pixel size of 6 mm, making it possible to image structures of 1.2 cm or larger. This is generally considered sufficient for most SPECT applications. The one exception is bone SPECT where a  $128 \times 128$  matrix may be used to take advantage of the higher counting statistics to improve spatial resolution.

### Arc of Rotation

As previously stated, a  $180^\circ$  acquisition is acceptable (right anterior oblique position to left posterior oblique position) for cardiac imaging since the myocardium is always in the near field of the detector(s). Photons traveling in a posterior direction from the myocardium must travel significant distances through tissue and, therefore, spatial resolution and sensitivity (due to attenuation) are degraded in posterior and right posterior oblique views. Thus, the data from the omitted projections are considered to be of poor quality and generally not acquired. For most applications, however, a  $360^\circ$  acquisition is required in order to obtain a complete set of projections for acceptable image reconstructions.

### Projections per Arc of Rotation

The same sampling theory previously described also applies to the determination of the number of projection views that should be acquired throughout an arc of rotation. With current instrumentation, 120 views are typically obtained with a  $360^\circ$  acquisition, and, therefore, 60 views are generally acquired with a  $180^\circ$  acquisition.

### Time per Projection

In general, SPECT techniques require the acquisition of as many photon events as possible in order to produce high-quality images. However, the limiting factor is typically the time that a patient can remain motionless during the acquisition. This is typically a period of 15–30 min and results in imaging times of 15–30 s for each projection when 120 projections are acquired in a  $360^\circ$  rotation. For cardiac applications, the imaging time is typically reduced to 10–15 min.

## ***SPECT Image Formation***

SPECT data are acquired in the form of multiple projection images as the scintillation camera heads rotate about the region of interest. Each acquired image is actually a set of count profiles measured from different views with the number of count profiles determined by the number of rows of pixels in the acquisition matrix (e.g., 64 for a  $64 \times 64$  matrix size). Using parallel hole collimators, each pixel is the sum of measured photon events traveling along a perpendicular ray and interacting at a point in the detector crystal represented by the pixel location. For a  $360^\circ$  acquisition with 120 acquired

projection arrays, 120 count profiles are acquired at  $3^\circ$  increments around the region of interest for each transaxial slice through the radionuclide distribution.

### Image Reconstruction

An image of a transaxial slice through the distribution can be generated by sequentially projecting the data in each count profile collected from the selected slice back along the rays from which the data were collected and adding the data to previously backprojected rays. The mathematical term for this process is the linear superposition of backprojections. Since there is no a priori knowledge of the origin of photons along each ray, the value of each pixel in the count profile is placed in each data cell of the reconstructed image along the ray. Representations of the images resulting from this process are shown in Fig. I.1.2. It should be noted that uniform projections are used in Fig. I.1.2 to illustrate the backprojection principle. In fact, the rays at the periphery of the sphere are of less intensity than at the middle. The classic “star effect” blur pattern inherent in backprojection images is also evident in these images with each ray of the star corresponding to one projection view. The importance of collecting the appropriate number of projections is evident from this diagram. Increasing the number of projections enhances the image contrast and reduces the potential for artifacts from the “star effect.” This can be seen in Fig. I.1.2D, where two additional sets of data at  $45^\circ$  and  $135^\circ$  are projected back into the image.

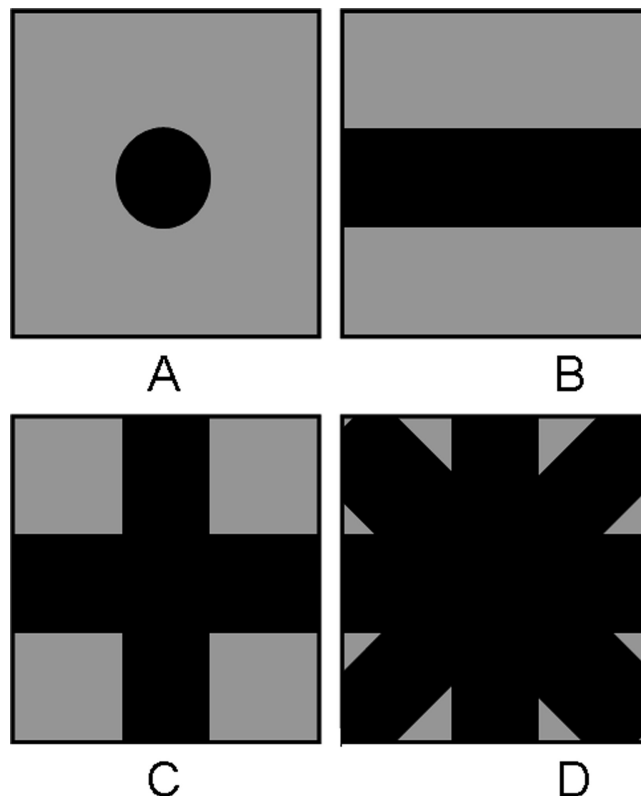


**Fig. I.1.2** A–D Examples of two filtered count profiles of data acquired at  $90^\circ$  from a spherical source and the resulting image distribution after backprojection of the filtered profiles (Reprinted with permission of Springer Science + Business Media from Vitola J, Delbeke D, eds. *Nuclear Cardiology and Correlative Imaging: A Teaching File*. New York: Springer-Verlag, 2004.)

It is apparent from the data in Fig. I.1.2 that the blur pattern inherent in backprojection results in a significant background that reduces image contrast. To reduce these effects and also to reduce the statistical effects of noise in the images, the mathematical technique of filtering is applied to the count profiles in the projection data before backprojection is performed. A filter is a mathematical function that is defined to perform specific enhancements to the profile data. In general, filters enhance edges (sharpen images) and reduce background. The effects of a simple edge enhancement filter are shown in Fig. I.1.3. In the application of this filter, each data point in the profile is replaced by a mathematical relationship between its value and those of adjacent data points. This relationship is designed such that negative values are added to the count profiles. Figure I.1.3 shows the backprojection of the filtered count profile at  $0^\circ$  added to the filtered backprojected count profile at  $90^\circ$ . It can be observed that the negative data at the edges of one profile cancel unwanted data from other profiles. This effect is shown diagrammatically in Fig. I.1.3B, C. As the number of projections is increased, this effect becomes more pronounced as shown in Fig. I.1.3D, where the filtered backprojections at  $45^\circ$  and  $135^\circ$  are added to the image. The final step is to set to zero each pixel in the reconstructed image that has a negative value as shown in Fig. I.1.3E. The figure shows that the scanned object is now visible in the image but many non-zero pixels remain. The addition of multiple projections will remove

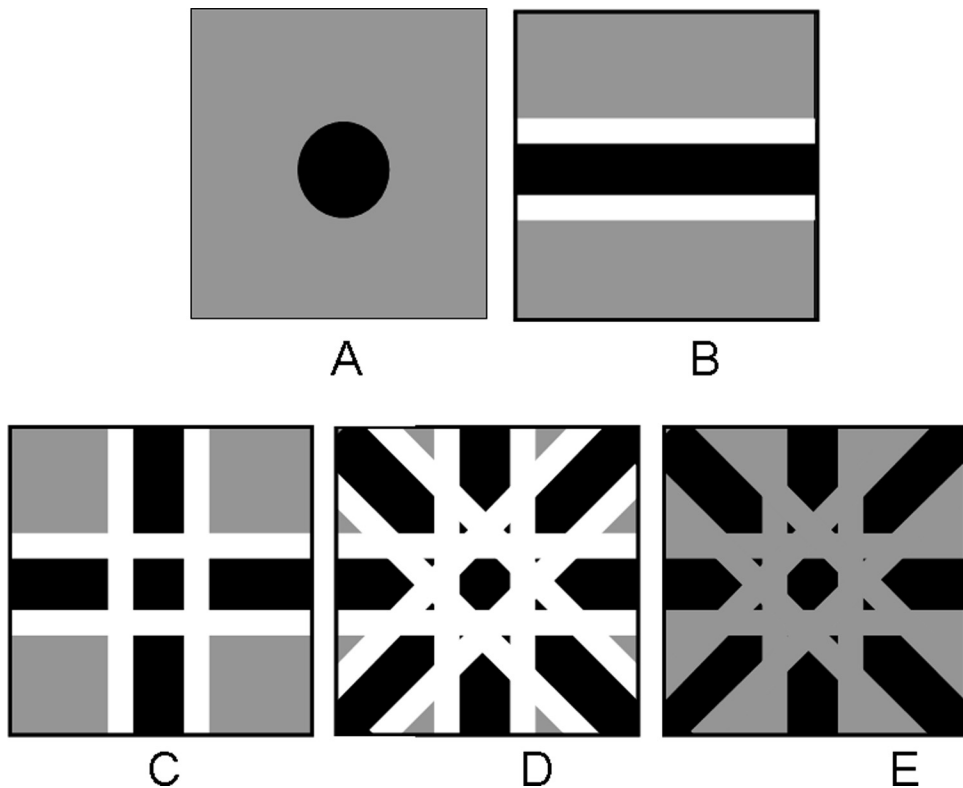


**Fig. I.1.3** Demonstration of the blur pattern from a spherical source (A) resulting from filtered back-projection of a single view (B), two views at  $0$  and  $90^\circ$  (C), and  $0$ ,  $45$ ,  $90$ , and  $135^\circ$  (D). In the final image (E) the negative values have been set to zero (Reprinted with permission of Springer Science + Business Media from Vitola J, Delbeke D, eds. *Nuclear Cardiology and Correlative Imaging: A Teaching File*. New York: Springer-Verlag, 2004.)

these artifacts and further enhance the image of the actual measured distribution. This technique of linear superposition of filtered backprojections has been the image reconstruction algorithm of choice throughout most of the history of SPECT. Figure I.1.3 also demonstrates the need to select an appropriate filter for each imaging application. If too many negative numbers are added to the image (over-filtering), valuable image data will be removed. If not enough negative numbers are added to the image (under-filtering), unwanted data will remain in the image resulting in artifacts. The selection of the appropriate filter is probably the most significant factor in producing a high-quality image reconstruction. The effect of over-filtering and under-filtering is shown in the single reconstructed slice of the myocardium of a patient in Fig. I.1.4.

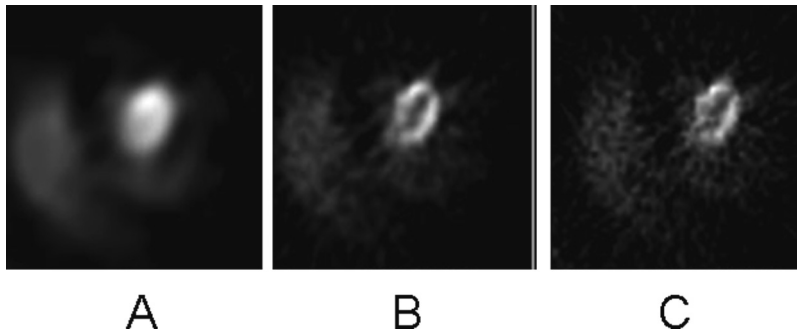


**Fig. I.1.4** Single short axis view of the myocardium with  $^{99m}\text{Tc}$  Sestamibi demonstrating over-filtering (A), under-filtering (C), and optimal filtering (B) (Reprinted with permission of Springer Science + Business Media from Vitola J, Delbeke D, eds. *Nuclear Cardiology and Correlative Imaging: A Teaching File*. New York: Springer-Verlag, 2004.)

The techniques previously discussed were illustrated using data for a single transverse slice. In practice, it is possible to reconstruct as many transverse slices as there are rows in the acquisition matrix. For example, a  $64 \times 64$  matrix provides 64 rows of data that can be used to reconstruct 64 slices. However, because the slice thickness of a single slice often exceeds the spatial resolution of the camera and the data in a single slice are often statistically limited, it is common practice to add two or more adjacent slices in order to reconstruct thicker slices with improved statistics. The final result of the reconstruction process is a set of transverse slices. Images of sagittal and coronal slices can easily be generated from this data set by simply reformatting the data. For the special case of the heart where its orientation is not in the traditional x, y, z orientation of the human body, it is necessary to re-orient the axes to correspond to the long and short axes of the left ventricle. This is a straightforward procedure that can be accomplished automatically or manually under software control.

## Filters

Routine methods for characterizing nuclear medicine images and data sets relate to the number of counts in a pixel. When data are referred to using this terminology, the data are defined as being in the *spatial domain* and the simple filter previously used to illustrate the effects of filtering on image reconstruction was a *spatial filter*. In practice, filtering of projection data in the spatial domain is often cumbersome and time consuming. This problem can be overcome by working in the *frequency domain*. Here, the projection data may be expressed as a series of sine waves, and a frequency filter may be used to modify the data. The conversion of the



projection data into the frequency domain is accomplished by the application of a mathematical function, the Fourier transform, and the result is that the projection data are represented as a frequency spectrum plotting the amplitude of each frequency in the data as shown in Fig. I.1.5A. In SPECT, this frequency spectrum has three distinct components. Background data (including the data from the star effect previously described) typically have very low frequencies and therefore are the main components of the low-frequency portion of the spectrum. Statistical fluctuations in the data (noise) generally have high frequencies and therefore dominate the high frequencies of the spectrum. True source data lie somewhere in the

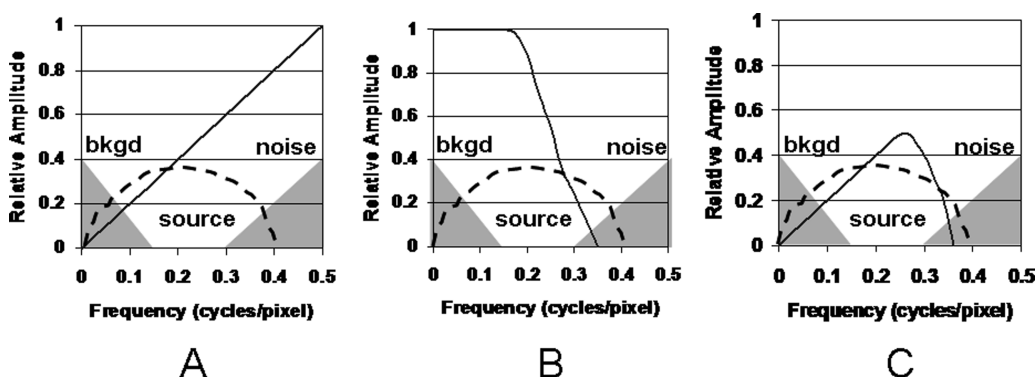


**Fig. I.1.5** In the frequency domain, image data can be represented as a series of sine waves, and the data can be plotted as a frequency spectrum showing the amplitude of each frequency. Image data have three major components: background, source information, and noise. A ramp filter is used to eliminate or reduce the contribution of background to the reconstructed image (A). A low-pass filter reduces the contribution of noise to the image (B). Combining the two filters (C) creates a window or band-pass filter that accepts frequencies primarily from the source distribution (Reprinted with permission of Springer Science + Business Media from Vitola J, Delbeke D, eds. *Nuclear Cardiology and Correlative Imaging: A Teaching File*. New York: Springer-Verlag, 2004.)

middle while overlapping the background and noise components of the spectrum. Thus, the challenge in filtering SPECT data is clearly demonstrated in Fig. I.1.5A. The goal is to eliminate background and noise from the data while preserving as much of the source data as possible. It should also be noted that the frequency data in the figure are plotted as a function of cycles/pixel. In the discussion of matrix size previously presented, the concept of the Nyquist frequency was introduced. In the frequency domain, the highest frequency in a data set occurs when one complete cycle covers two pixels. Frequencies higher than this value cannot be imaged. This fact translates into a frequency of 0.5 cycles/pixel as the frequency limit and is defined as the Nyquist frequency. This is why the plot in Fig. I.1.5A terminates at 0.5 cycles/pixel. The pixel size used in a particular application can be introduced into this definition so that the Nyquist frequency for the application can be determined. For example, a pixel size of 0.5 cm would define a Nyquist frequency of 1.0 cycles/cm. And the smallest object size that could possibly be resolved in an image would be 1 cm.

The first step in filtering is to design a filter to remove or reduce the background. This typically is a ramp filter as shown in Fig. I.1.5A, a high-pass filter that reduces only the amplitudes of low-frequency data while having no effect on the mid-range and high-frequency data which contain the detail in the source (and also the noise). The second step is to define a filter to remove or reduce the noise while preserving the detail in the source



data. This is accomplished using a low-pass filter as shown in Fig. I.1.5B, which accepts selected frequencies up to a certain value. There are a number of low-pass filters that are available for processing SPECT data. Some have fixed characteristics, and others have flexibility in choosing the cutoff frequency and/or the slope of the filter. Some filters are optimized for image data with excellent counting statistics, and others provide the capability for filtering data with poor statistics. Also, the amount of detail in an image and the object sizes to be resolved (spatial resolution) are important factors to be considered in the selection of a filter. In practice, the low-pass filter may be applied first to reduce the effects of noise, and then the ramp filter is applied to reduce background. The two filters may be combined as shown in Fig. I.1.5C to function as a band-pass filter. It can be seen in the latter figure that appropriate selection of the cutoff frequency will eliminate much of the noise, and selecting an appropriate filter shape will preserve most of the source data. The terms under-filtering and over-filtering were previously referenced, and examples were shown in Fig. I.1.4. From Fig. I.1.5C, it can be observed that, when a cutoff frequency is chosen that is too low, some of the source data will be excluded from the final image, and this situation is referred to as over-filtering. Similarly, when too high a cutoff frequency is chosen, excessive noise will be included in the final image, and this is referred to as under-filtering. In clinical applications, most imaging systems provide the capability for trying different filters and filter parameters on a single slice of image data in order to select the appropriate processing algorithm for a specific patient study. Technologists and physicians in the clinical setting often prefer this method of trial and error.

### Iterative Reconstruction

Filtered backprojection amplifies statistical noise, which adversely affects image quality. To address this problem, Shepp and Vardi introduced an iterative reconstruction technique in 1982<sup>10</sup> based on the theory of expectation maximization (EM), which has a proven theoretical convergence to an estimate of the actual image distribution that has a maximum likelihood of having projections most similar to the acquired projections. The initial implementation of these algorithms was very time consuming, with several iterations being required to reach a solution, and extensive computer power was required. Since that time, much effort has been expended in improving and testing algorithms based on this concept. Significant improvements in speed and signal-to-noise and reconstruction accuracy have resulted from these efforts. In 1994, Hudson and Larkin<sup>11</sup> developed the technique of ordered sets EM (OS-EM) for image reconstruction from 2D projection data. This algorithm was based on the concept of dividing the projection data into small subsets (e.g., paired opposite projections in SPECT data) and performing the EM algorithm on each subset. The solution of each subset was used as the starting point for the next subset, with subsequent subsets being selected to provide the maximum information (e.g., chose the second subset of data to be orthogonal to the first subset). The advantage of this technique is that, at the end of the first pass, the entire data set has been processed one time, but  $n$  successive approximations to the final solution have been made where  $n$  is the number of subsets. Thus, OS-EM is  $n$  times faster than the original EM algorithm. Typically, only two to three passes through the data set (iterations) are required for the reconstructed image to converge to a final value that is essentially unchanged by further iterations. Correction for scatter and attenuation effects (topics that will be discussed later) can be performed on the acquired projection data during the reconstruction process. The advantage of this technique is that the star effect inherent in filtered backprojection is virtually eliminated since the acquired data are distributed within the body contour. Because of this

result, signal-to-noise is generally improved. Filtering of the data can also be performed to further enhance the reconstructed images.

### Attenuation Correction

One of the primary factors affecting image quality in SPECT is photon attenuation. Photons are attenuated in the body due to photoelectric absorption and Compton scatter, with Compton scattering being the most predominant interaction in the diagnostic energy range. The probability of Compton scattering decreases with increasing energy. The effects of attenuation are significant, with approximately 62% of 70 keV photons and 54% of 140 keV photons being attenuated in 5 cm of tissue. Photoelectric absorption results in a complete removal of the photon from the radiation field, while Compton scattering results in a change in direction with loss of photon energy, the magnitude of the loss being determined by the angle of scatter. Thus, Compton scattered photons enter the camera crystal with minimal or no information on their origins due to their change in direction within the patient. Pulse height analysis is used to prevent the counting of photons that have scattered through large angles (greater loss of energy), but small angle scattered photons are counted. The use of a 20% window at 70 keV permits the acceptance of photons that have scattered through 0–79°. At 140 keV, a 20% window permits the acceptance of photons that have scattered through 0–53° and a 15% window accepts photons scattered through 0–45°.

Correction of images for attenuation effects are complicated by the broad range of tissue types (lung, soft tissue, muscle, and bone) that may reside in the region of interest resulting in a non-uniform attenuation medium. A commercial approach to attenuation correction that has been used in the past used line sources of  $^{153}\text{Gd}$  as shown in Fig. I.1.6. These sources provide beams of 100 keV photons and are scanned in the longitudinal direction at each step of the SPECT acquisition to provide transmission maps of the region under study. Emission and transmission scans at each step can be acquired sequentially or simultaneously using

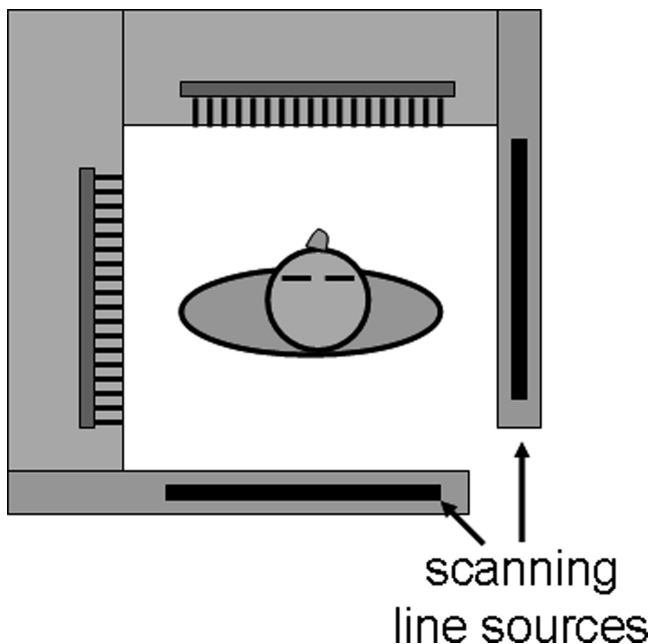


**Fig. I.1.6** Scanning line sources mounted on a dual-head, 90° geometry scintillation camera for attenuation correction measurements (Reprinted with permission of Springer Science + Business Media from Vitola J, Delbeke D, eds. *Nuclear Cardiology and Correlative Imaging: A Teaching File*. New York: Springer-Verlag, 2004.)

synchronized energy windows that move with the sources to acquire the transmission data. These are then used to correct the projection data prior to SPECT image reconstruction.

Correction methods tend to overcorrect for attenuation, and it is generally accepted that a scatter correction must also be performed. One solution to this problem is the simultaneous acquisition of a second set of planar projections using a scatter window positioned just below the photopeak energy being measured. This window is used to determine correction factors for the acquired planar projections prior to image reconstruction.

## Positron Emission Tomography

Previous discussions have been related to the imaging of single photon emitting radionuclides using conventional scintillation camera systems. Another classification of radionuclides that have applications in nuclear medicine is positron emitters that can be imaged using specially designed PET systems optimized for the unique decay properties of these radionuclides. Anger and Rosenthal<sup>1</sup> originally proposed the use of the scintillation camera for this application, and throughout the years numerous attempts have been made to use this instrument for this application.<sup>12,13</sup> However, these approaches suffered from deficiencies in the efficiency of NaI(Tl). Robertson and coworkers<sup>14</sup> and Brownell and Burnham<sup>15,16</sup> developed special purpose positron imaging systems in the early 1970s, but the modern day PET scanner began to evolve in 1975<sup>17</sup> with the work of Phelps and his associates producing a system of detectors operating in coincidence mode and surrounding the patient to provide transverse section imaging capabilities.<sup>18–22</sup> Positron emitting radionuclides are distinguished by the unique method by which they are detected. The positron is a positively charged electron. When emitted from a radioactive nucleus, it travels only a very short distance before losing all of its energy and coming to rest. At that instant, it combines with a negatively charged electron, and the masses of the two particles are completely converted into energy in the form of two 511 keV photons. This process is termed *annihilation*. The two annihilation photons leave the site of their production at 180° from each other. This process can be detected as shown in Fig. I.1.7 by using small, dual-opposed detectors connected by a timing circuit, termed a *coincidence* circuit, to simultaneously detect the presence of the two annihilation photons, a signature of the positron decay process.

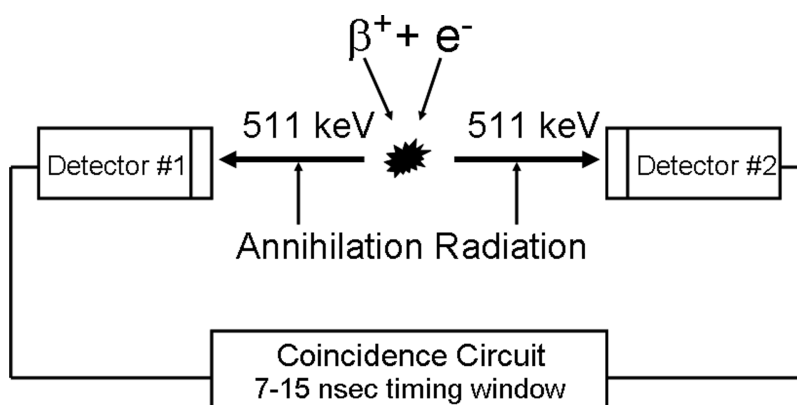


**Fig. I.1.7** Block diagram of a two-detector grouping with a coincidence timing window used to simultaneously detect the two photons resulting from the annihilation of a positron–electron pair using the technique of coincidence counting (Reprinted with permission of Springer Science + Business Media from Vitola J, Delbeke D, eds. *Nuclear Cardiology and Correlative Imaging: A Teaching File*. New York: Springer-Verlag, 2004.)

The timing window must be small, 7–15 ns, in order to reduce the possibility of detecting photons from two separate decay processes, i.e., random events. The spatial resolution of the imaging system is primarily determined by the size of the detectors, combined with the uncertainty due to the travel of the positron before annihilation which is typically less than 0.5 mm in tissue. In clinical imaging systems, many small detectors are used in multiple rings to provide high sensitivity for detection in the region being examined as shown in Fig. I.1.8.

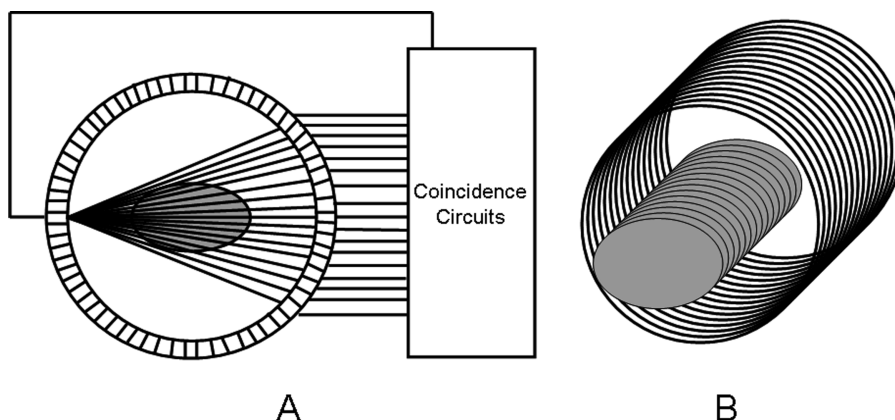


**Fig. I.1.8** One ring of detectors from a multi-ring PET system. Many potential lines of coincidence are possible for each detector in the ring (A). Multiple rings of detectors are used to extend the axial field of view (B) (Reprinted with permission of Springer Science+Business Media from Vitola J, Delbeke D, eds. *Nuclear Cardiology and Correlative Imaging: A Teaching File*. New York: Springer-Verlag, 2004.)

### **PET Detectors**

For many years, the scintillation detector of choice for PET imaging has been bismuth germanate (BGO) instead of NaI(Tl), which is used in other nuclear medicine imaging devices. BGO is used because of its high-density and high effective atomic number, which results in a high intrinsic detection efficiency for 511 keV photons. A 30-mm thick crystal of BGO has an intrinsic detection efficiency of approximately 90% at 511 keV. When two detectors are used in coincidence to simultaneously detect two 511 keV photons, the coincidence detection efficiency is the product of the efficiencies of the two detectors or approximately 81%. Recently, a new scintillation material, lutetium oxyorthosilicate (LSO), has been introduced as a possible replacement for BGO. Although currently more expensive than BGO, LSO has the advantage of greater light output (factor of 6) and faster decay time (factor of 7.5), and these improvements can be used to advantage in increasing the count rate capabilities of modern day systems. PET systems using LSO are now available from one manufacturer (Siemens-CTI). More recently, another new scintillation detector material, gadolinium oxyorthosilicate (GSO) has been introduced with similar characteristics to those of LSO, but with improved energy resolution. PET systems using GSO detectors are now available from another manufacturer (Philips Medical Systems).

The high spatial resolution of these systems is accomplished by using a unique combination of small crystals and photomultiplier tubes. An example of this technology is shown in Fig. I.1.9. A rectangular solid crystal of detector material is modified by the addition of vertical and

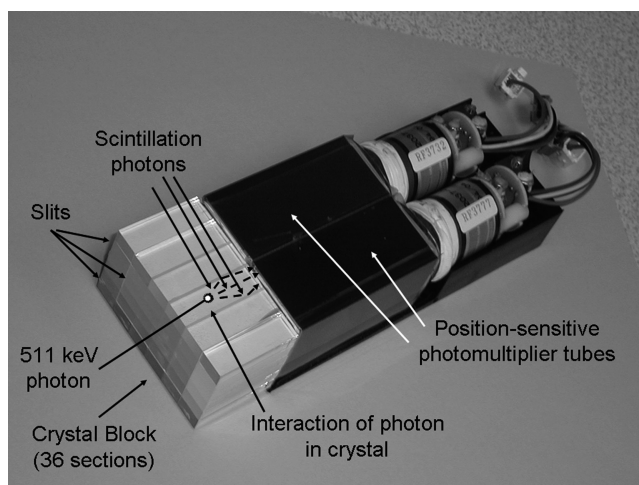


**Fig. I.1.9** For high-resolution imaging, a block of crystal (BGO in this example) is segmented into many small discrete detectors (32 in this example). Two position-sensitive photomultiplier tubes positioned at the back of the crystal block determine the detector in which an interaction occurs (Reprinted with permission of Springer Science + Business Media from Vitola J, Delbeke D, eds. *Nuclear Cardiology and Correlative Imaging: A Teaching File*. New York: Springer-Verlag, 2004.)

horizontal grooves partially through the volume to effectively create a block of many small discrete detectors (36 in the figure). Some manufactures actually separate the discrete crystals entirely, creating pixilated detectors as in the figure. A photon interaction in one of the discrete crystals will result in scintillations localized primarily in that crystal. The crystal in which the interaction occurred is then identified by photomultiplier tubes using conventional Anger logic and mounted on the base of the crystal block or by using position-sensitive photomultiplier tubes. In the detector block shown in Fig. I.1.10, the discrete crystals are

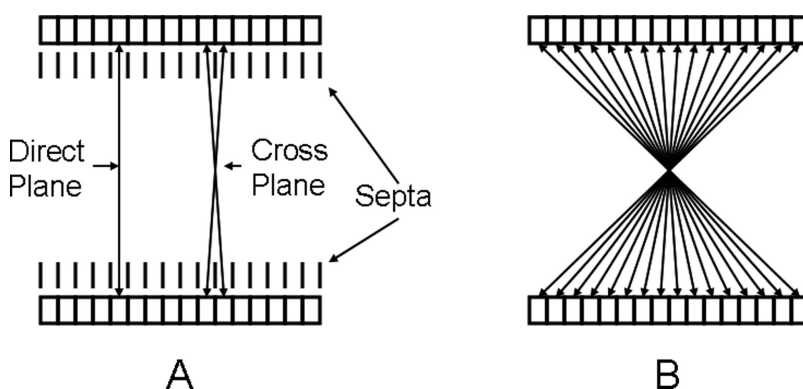


**Fig. I.1.10** The use of septa collimators permit 2D acquisition by limiting the detection of coincidence events to detectors within a single ring (direct planes) and detectors in adjacent rings (cross planes) (A). When the septa are withdrawn, 3D acquisition is established by permitting the measurement of a coincidence event in two detectors in any two rings of the system (B) (Reprinted with permission of Springer Science + Business Media from Vitola J, Delbeke D, eds. *Nuclear Cardiology and Correlative Imaging: A Teaching File*. New York: Springer-Verlag, 2004.)

4 mm  $\times$  8 mm  $\times$  30 mm deep, resulting in a transaxial spatial resolution of 4.6 mm. Current systems have 18–32 rings of detectors providing axial fields of view of 15–18 cm (Fig. I.1.8). Thus, the imaging of sections of the body greater than 15 cm in the axial direction requires multiple acquisitions obtained by indexing the patient through the system using a movable imaging table under precise computer control.

## ***2D Versus 3D Imaging***

It is possible to reduce the effects of scatter and the possibility of random events by adding thin 1D collimators, termed septa, between adjacent rings of detectors to shield the detection of events in the axial direction as shown in Fig. I.1.10A. These septa are typically constructed from tungsten with a thickness of 1 mm and spacing to match the axial width of each discrete crystal. They have the effect of creating 2D slices from which events can be accepted in any transaxial direction. Thus, for a system with 18 rings of detectors, 18 direct imaging planes are established. To increase sensitivity, coincidence circuitry can also be used to record interactions occurring in two detectors in adjacent rings, resulting in the addition of a new acquisition plane positioned midway between the adjacent detector rings. Thus, in an 18-ring system, 17 new cross imaging planes can be added for a total of 35 imaging planes in this example. Additional sensitivity is obtainable by adding adjacent planes to this process. For example, three or five planes of detectors may be electronically grouped so that coincidence events may be measured in any two detectors within these groupings. The localization of the coincidence event in a transaxial imaging plane is typically determined by averaging the axial positions of the two detectors. The length of the septa limits the axial separation of any two rings that can actually be used in the measurement of the activity in a 2D plane.

With the septa retracted or in systems using only 3D technology, detector rings are opened to photons traveling in all directions, and a 3D imaging geometry is established as shown in Fig. I.1.10B. This increases the system sensitivity by a factor of 3–5 over that of 2D imaging. However, the randoms rate and scatter fraction are increased with this geometry, which may reduce contrast. It is possible to limit the acceptance angle in the axial direction to reduce the effects of randoms and scatter, but this process results in a reduction in sensitivity.

## ***Data Acquisition and Image Reconstruction***

As previously described, a coincidence event is recorded when two photons are simultaneously measured in two separate detectors. Thus, the coordinates of the two detectors determine the line of response (LOR) defined by the coincidence detection of the two photons as shown in Fig. I.1.11A. These coordinates are captured by calculating the perpendicular distance from the center of the scan field to the LOR ( $r$ ) and measuring the angle between this line and the vertical axis ( $\phi$ ). These coordinates are then recorded as a data point in an ( $r, \phi$ ) plot or sinogram as shown in Fig. I.1.11B. Each unit in the final sinogram will consist of the total number of coincidence events recorded by a two-detector pair. The sinogram method of storage is used because it is more efficient than the storing of list mode data that record individual coordinates of detector pairs. In 2D image acquisition, there will be  $(2n - 1)$  sinograms recorded, one for each direct plane



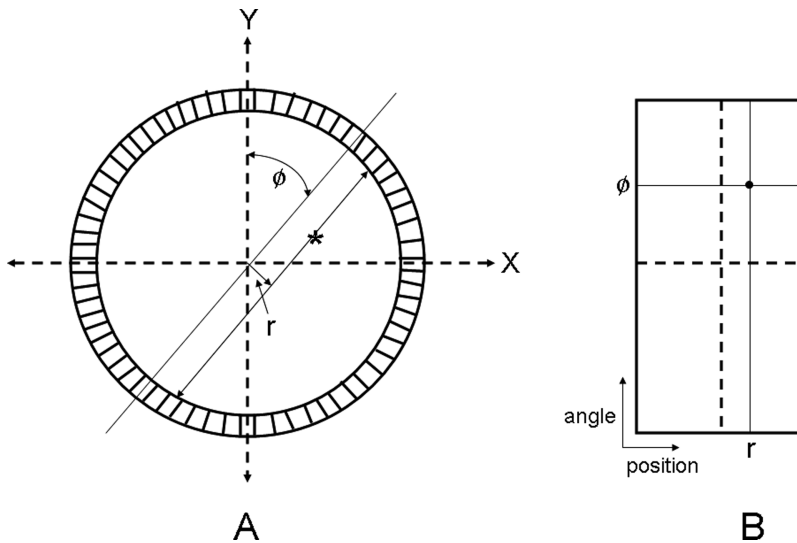


**Fig. I.1.11.** The coordinates of the two detectors involved in a coincidence measurement are captured by calculating the perpendicular distance from the center of the scan field to a line connecting the two detectors ( $r$ ) and measuring the angle between this line and the vertical axis ( $\phi$ ) (A). These coordinates are then recorded as a data point in an ( $r, \phi$ ) plot or sinogram (B). Each unit in the final sinogram will consist of the total number of coincidence events recorded by a two-detector pair (Reprinted with permission of Springer Science + Business Media from Vitola J, Delbeke D, eds. *Nuclear Cardiology and Correlative Imaging: A Teaching File*. New York: Springer-Verlag, 2004.)

and one for each cross plane, where  $n$  is the number of detector rings in the PET system. When the two detectors are in different detector rings, the event is recorded in the sinogram corresponding to the average axial position of the two rings as previously stated.

Image reconstruction of the 2D data is accomplished by first converting each sinogram of data into a set of planar projections. This can be accomplished in a straightforward manner from the sinograms since each horizontal row of data in a sinogram represents events recorded at one angular position. It should also be noted that the events from each two-detector pair are uniformly spread across the sinogram. As described in the section on SPECT reconstruction, a filtering algorithm is applied to each projection, after which the data are projected back along the lines from which they were acquired to generate the final image (i.e., filtered backprojection). Each sinogram of data is used in this fashion to generate an image corresponding to the activity distribution represented by the sinogram. Iterative algorithms that make use of ordered sets (OS-EM) can also be used in the 2D reconstruction process to reduce noise and provide high-quality images.<sup>4</sup> The use of iterative algorithms also simplifies the process of adding corrections for effects such as attenuation and scatter.

The acquisition and reconstruction of 3D data sets are more complicated than that for 2D applications. First, it is not possible to perform the axial averaging of events recorded from two detectors in different detector rings. The origins of these data must be preserved in the acquisition process, and this results in a significant increase in the size of the acquired data set since  $n^2$  sinograms are now required to accurately acquire the data. In addition, the reconstruction process is complicated by the fact that it is necessary to use a true 3D volume



algorithm to accurately locate detected events in axial as well as transverse directions. Iterative reconstruction algorithms, although very time consuming and labor intensive, are well designed for this application. Currently, available systems offer this technique as an option, and it has proven useful in brain imaging because the imaging volume is relatively small and count rates are relatively low. Because of the added sensitivity provided by 3D imaging, a great deal of effort has been applied to develop accurate and efficient 3D algorithms and techniques to correct for scatter in order to improve contrast. These improvements have resulted in the 3D technique becoming the most prevalent choice for clinical PET imaging.

### ***Time-of-Flight PET***

In conventional PET, the localization of a positron decay and the resultant production of annihilation radiation are represented by a LOR between the two detectors that detect the two annihilation photons. There is no way of identifying the precise position along the LOR where the decay process occurred. For many years, investigators have worked to solve this problem by using time-of-flight (TOF) techniques, but they have been limited by the response time of the detectors and the technology of timing measurements that have been available. The availability of fast LSO crystals and improvements in timing measurement capability now make the application a reality. Instead of using conventional timing circuitry to identify coincidence events within a timing window, TOF PET uses more sophisticated timing circuitry to measure the time difference between the detection of the two photons from an annihilation event. Since the photons travel at a known velocity, the speed of light ( $c$ ), this time difference can be used to calculate the difference in distance of travel of the two photons between the two detectors involved in the measurement. Using this measurement and the known distance between the two detectors, the actual distance of travel of the two photons can be calculated (and therefore the location of the annihilation event). Current timing resolutions on the order of 0.6 ns yield an uncertainty on the order of 9 cm in the measurement of the location of the annihilation event. Thus, the conventional LOR between the two detectors is replaced with a LOR of approximately 9 cm whose center is the estimate of the location of the annihilation event.

The use of TOF PET technology results in improved contrast and spatial resolution by significantly reducing the uncertainty in the actual location of the annihilation event. Although signal processing is more intensive with this technology, improvements in lesion detection and image quality have been demonstrated in a commercial system using TOF technology, especially in large patients where random and scatter events are more prevalent.

### ***Quantitative Techniques***

Because of the block detector technology used with PET systems, there is a dead time associated with measurements of activity distributions, and corrections for this effect must be implemented in order that the measurements are quantitatively accurate. When an interaction occurs in a crystal, a finite length of time is required to collect the light produced and process the resulting signal. If another event occurs in the same block while the first interaction is being processed, the light from the two events will be summed together by the photomultiplier tubes in that block, and the resulting signal will probably fall outside of the pulse height window. This effect will result in an

erroneous measurement of count rate. Modern systems have dead time correction capability utilizing correction factors determined for the system as a function of count rate. These correction factors adjust for errors in count rate but cannot add the lost events back into the acquired image.

A state-of-the-art PET scanner may have several thousand discrete crystals coupled to hundreds of photomultiplier tubes. Thus, there are inherent differences in sensitivity between detector pairs in the measurement process, and it is necessary to correct for these differences in order for measurements of coincidence events to correspond to the activity distribution being imaged. This correction is generally accomplished by exposing each detector pair to a uniform source distribution, typically created by a rotating rod source of  $^{68}\text{Ge}$  and measuring the response of each detector pair. This data set is called a blank scan. The blank scan can be used to create normalization factors that are stored away and used to correct data subsequently acquired in image acquisition. Blank scans must be acquired frequently (at least weekly) in order to monitor system parameters and adequately correct for small changes in detector responses.

A second factor to be considered is the exponential attenuation of photons within the body. Photons are either absorbed or scattered by tissues based on the attenuation coefficients of these tissues and the distance of travel through the body. The attenuation effects are much more significant in coincidence imaging than in single photon imaging since both photons from a single annihilation process must pass through the body without interaction in order to be detected and counted as a coincidence event. The probability of this occurrence is much less than that for a single photon emitted from the same location to escape the body without interaction. These effects result in non-uniformities, distortions of intense structures, and edge effects. Therefore, it is necessary to correct for attenuation to eliminate these effects, especially in the thorax and abdomen where attenuation is non-uniform due to the presence of different tissue types. Since the brain is relatively uniform, it is possible to perform a calculated attenuation correction. This is accomplished by outlining the outer contour of the head, assuming uniform attenuation within this volume, and calculating correction factors to be applied to the raw projection data.

In the thorax and abdomen, because of the non-uniform attenuation, it is necessary to perform a measured attenuation correction. This approach is very accurate because attenuation of two annihilation photons from an annihilation event is independent of the location of the event. The total distance traveled through the patient is constant as shown in Fig. I.1.12A–C. It is therefore possible to measure the attenuation using an external source as shown in Fig. I.1.12D. In the past, this was typically accomplished by transmission scanning using a rotating rod source of  $^{68}\text{Ge}$  as in the acquisition of a blank scan for detector normalization, but with the patient present in the scan field. The transmission data can then be used to correct the raw projection data during the reconstruction process. Iterative reconstruction algorithms can be easily adapted to handle the attenuation correction process. Transmission scans with high counting statistics are required in order to prevent the addition of statistical noise in the corrected images. In the past, it was necessary to perform the transmission scan prior to administration of the radiopharmaceutical into the patient. This resulted in lengthened studies and the need for careful repositioning of the patient before acquiring the emission scan. More recent improvements in count rate capabilities have made it possible to acquire transmission scans after the patient has been injected with a radiopharmaceutical by increasing the activity in the transmission source. It

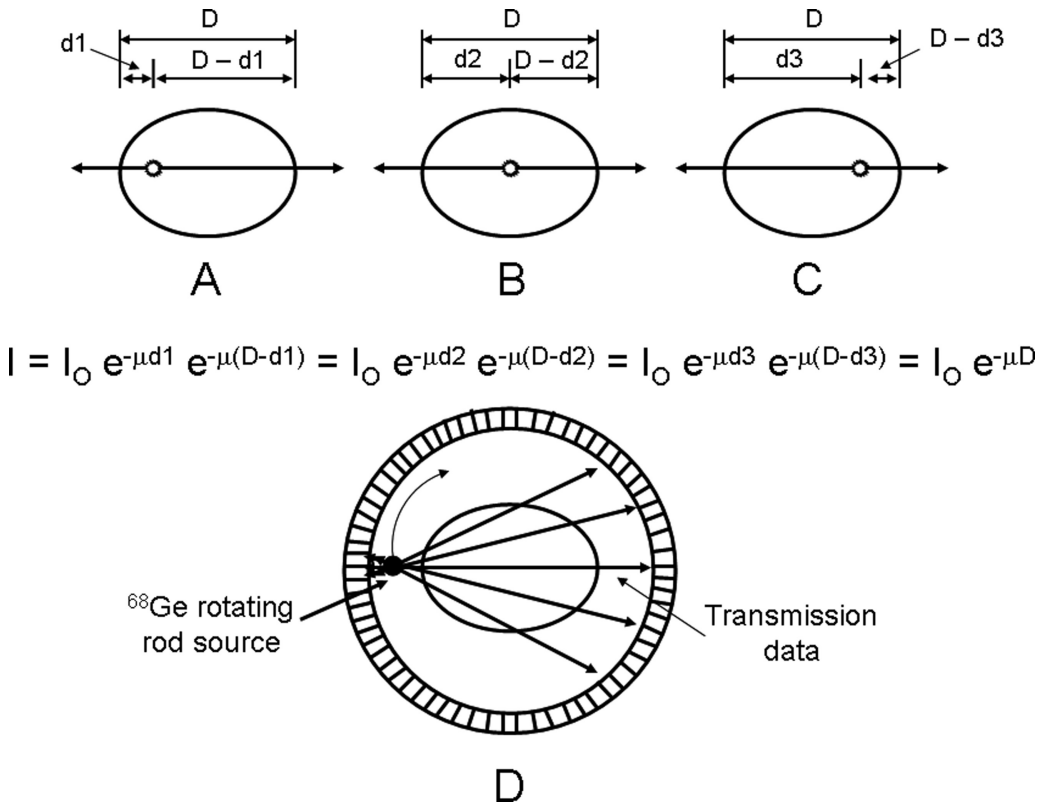


**Fig. I.1.12** The attenuation of two annihilation photons is independent of the location at which the two photons were produced, since the photon pair must always travel the same distance within the patient and escape without interaction in order to be detected as a true event (A–C). Thus, attenuation can be measured using a rotating rod source of a positron emitter such as  $^{68}\text{Ge}$  (D) (Reprinted with permission of Springer Science + Business Media from Vitola J, Delbeke D, eds. *Nuclear Cardiology and Correlative Imaging: A Teaching File*. New York: Springer-Verlag, 2004.)

has also been shown that it is possible to shorten the length of the transmission scan by using a process called segmented attenuation correction. In this process, attenuation coefficients are predetermined (based on certain tissue types) and limited in number. The measured attenuation coefficients from the transmission scan are then modified to match the closest allowed coefficients from the predetermined options. Figure I.1.13 shows a single coronal view reconstructed from a set of transmission scans, the corresponding view reconstructed from emission data using filtered backprojection, and the same view reconstructed using an OS-EM algorithm with attenuation correction.

The addition of transmission scanning permits accurate delineation of body contours. This fact makes it possible to limit image reconstruction to the areas defined by the contours. In addition, accurately knowing these contours permits the development of mathematical models for determining the contribution to the images of random and scatter events, and subsequently the implementation of correction methods to eliminate their effect. Work is currently ongoing in this area.

In order to make absolute measurements of activity in a region of the body, one additional calibration is necessary. A cylindrical phantom containing a very accurately

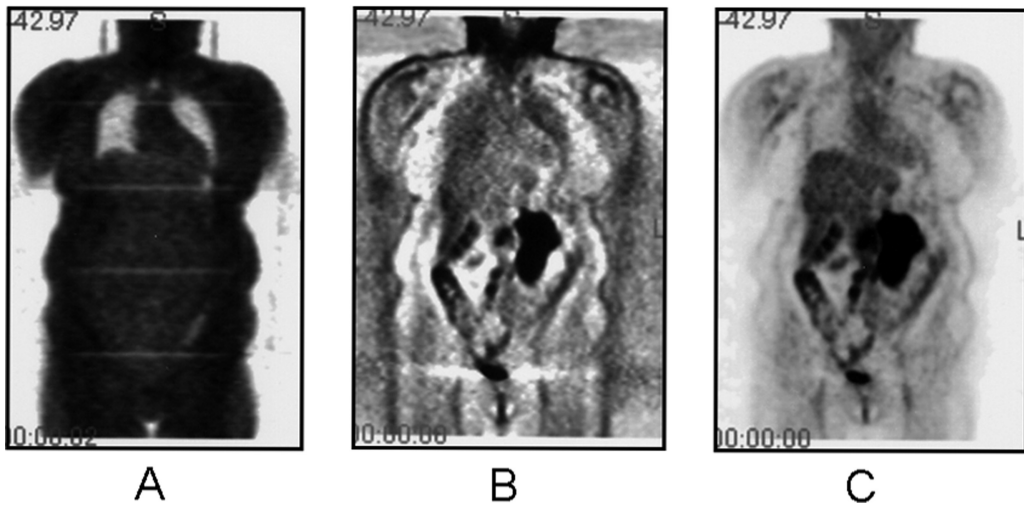


**Fig. I.1.13** (A) A coronal view of a transmission data set acquired from a multi-ring PET scanner. (B) A coronal view of a patient with gastric cancer imaged with  $^{18}\text{F}$ -FDG. The image was reconstructed without attenuation correction using filtered back projection. (C) The same coronal view of the  $^{18}\text{F}$ -FDG distribution reconstructed with attenuation correction from the transmission data set shown in (A) using an iterative reconstruction algorithm (OS-EM) (Reprinted with permission of Springer Science + Business Media from Vitola J, Delbeke D, eds. *Nuclear Cardiology and Correlative Imaging: A Teaching File*. New York: Springer-Verlag, 2004.)

known distribution of activity is scanned and total counts (after attenuation correction) are determined. A quantitative calibration factor is then determined by dividing the measured counts per unit time by the concentration of activity in the phantom. This results in a calibration factor of counts/s per  $\mu\text{Ci/cc}$ . To determine activity in a specific area, a region of interest is identified and the counts in the region are determined and converted to a count rate using the scan time, and the calibration factor is then used to calculate  $\mu\text{Ci/cc}$  in the region. Current systems have the capability of measuring absolute activity to within 5%. In practice, it should be noted that the same acquisition and reconstruction algorithms (and filters) should be used in acquiring and processing the phantom data and the patient data in order to obtain accurate quantitative data. A quantitative measurement that has proven to be of use in some clinical applications is the standard uptake value (SUV). This factor is determined by normalizing the measured activity in a region to the administered activity per unit of patient weight. Using the SUV, regions of abnormal uptake can be compared to that of normal regions, and lesion uptake in serial scans can be compared.

## X-Ray Computed Tomography

As described in the Introduction, SPECT and PET imaging technologies often suffer from insufficient anatomical detail. These deficiencies can be resolved by incorporating the techniques of x-ray CT into the image acquisition and reconstruction process. This technology was introduced to the medical community in the early 1970s when Hounsfield and Ambrose<sup>23</sup> introduced a computerized x-ray tube-based tomographic scanner using reconstruction algorithms developed by McCormack<sup>24</sup> to provide images of tissue densities from acquired

projections. CT scanning provides high quality and high spatial resolution ( $\sim 1$  mm) images of cross-sectional anatomy and therefore provides a significant portion of the anatomical images acquired in oncological applications, not only for diagnosis and staging of disease but also for simulations used for radiation treatment planning. CT images generally have a high sensitivity for lesion detection, but may have limited specificity in some applications. CT images are acquired as transmission maps with a high photon flux and are actually high-quality representations of tissue attenuation and thus can provide the basis for attenuation correction.

CT images are acquired by using a high-output x-ray tube and an arc of detectors in a fixed geometry to acquire cross-sectional transmission images of the patient as the x-ray tube and detectors configuration rapidly rotates around the patient as shown in Fig. I.1.14A, B. Current technology using multi-detector arrays and helical (spiral) scanning permits the simultaneous acquisition of as many as 64 thin slices (0.625 mm) in as little as 0.35 s. [If the rotation is 0.35 s, only a little more than half of the rotation is actually required to produce images.] The geometry of these third generation CT scanners results in the acquisition of transmission data in a fan beam geometry. However, each ray in a fan beam geometry can be represented by an equivalent ray in a parallel beam geometry.

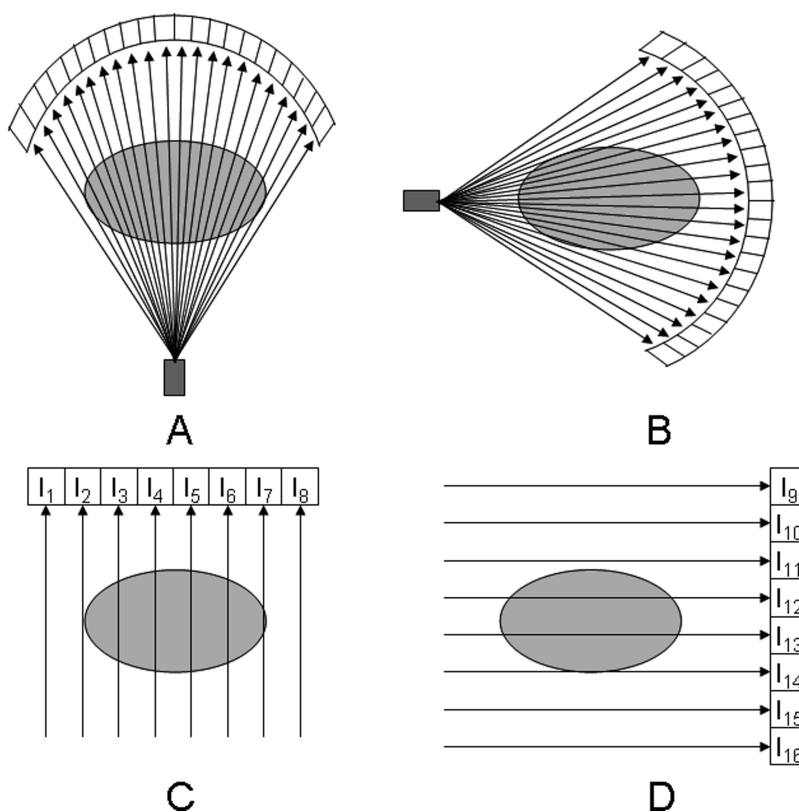


**Fig. I.1.14** CT data are acquired in a fan beam geometry where individual rays represent transmitted photon intensities from multiple projections around the patient (A, B). These data can be reformatted into an orthogonal geometry similar to that used for SPECT (C, D) (Reprinted by permission of the Society of Nuclear Medicine from: James A. Patton and Timothy G. Turkington. SPECT/CT Physical Principles and Attenuation Correction. *J Nucl Med Technol* 2008 36(1):1–10. Fig. 4.)

Therefore, a common approach is to convert the fan beam data to parallel beam geometry as illustrated diagrammatically in Fig. I.1.14C, D, in order to simplify the reconstruction process. This redistribution of data results in orthogonal data sets similar to that obtained from PET and SPECT. As many as 600 projection arrays are acquired in this manner in order to produce a high-quality transmission measurement of each slice of tissue.

Each measured ray ( $I$ ) is the initial ray intensity ( $I_0$ ) attenuated by a factor

$$I = I_0 e^{-\sum_i x_i \mu_i}$$

where the index  $i$  represents all the different tissue type regions along the trajectory,  $\mu_i$  are the effective attenuation coefficients for the different tissue regions, and  $x_i$  are the corresponding thicknesses of the tissue regions, so that the sum represents the total attenuation through all regions. With filtered backprojection (or another tomographic reconstruction technique), these attenuation measurements obtained, along all rays at all angles, are used to produce cross-sectional arrays of tissue attenuation coefficients as shown in Fig. I.1.15A. The resulting arrays are high-quality images of body attenuation and therefore representative of body anatomy. In order to standardize the data and provide sufficient gray scale for display, the data are typically converted to CT numbers (Hounsfield units) as shown in Fig. I.1.15B by normalizing to the attenuation coefficient of water using the following equation:

$$\text{CT number} = [(\mu_{\text{tissue}} - \mu_{\text{water}}) / \mu_{\text{water}}] \times 1000.$$

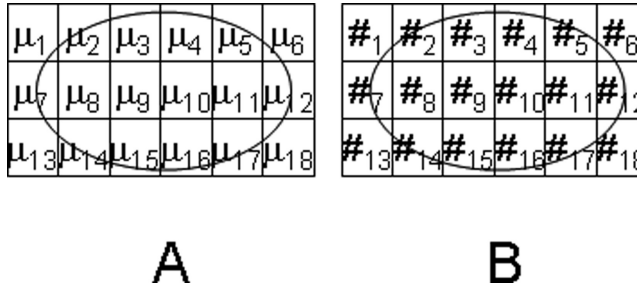


**Fig. I.1.15** The transmitted intensities can be used to solve for attenuation coefficients ( $\mu$ ) by using the unattenuated intensity ( $I_0$ ) by the attenuation equation ( $I = I_0 e^{-\mu x}$ ). Using filtered backprojection, an array of attenuation coefficients for each anatomical slice can be determined (**A**) and converted to an array of CT numbers for display purposes (**B**) (Reprinted by permission of the Society of Nuclear Medicine from: James A. Patton and Timothy G. Turkington. SPECT/CT Physical Principles and Attenuation Correction. *J Nucl Med Technol* 2008 36(1):1–10. Fig. 5.)

Based on this convention, the CT numbers of air and water are  $-1000$  and  $0$ , respectively. These images are typically displayed as  $256 \times 256$  or  $512 \times 512$  arrays, with pixels representing  $0.5$ – $2$  mm of tissue, because of the high spatial resolution inherent in the measurements.<sup>25,26</sup>



## ***SPECT/CT and PET/CT***

The integration of an emission tomography system (SPECT or PET) with a transmission tomography system (CT) into a single imaging unit sharing a common imaging table provides a significant advance in technology. Lang, Hasegawa, and colleagues<sup>27</sup> developed a prototype SPECT/CT imaging system using an array of solid-state detectors to acquire both the emission and transmission data. They subsequently integrated a commercial CT scanner and single-head SPECT camera to acquire sequential SPECT and CT scans using a common imaging table.<sup>28</sup> This work led to the introduction of the first commercially available SPECT/CT system.<sup>29</sup> At the same time, Townsend and colleagues integrated a commercially available PET scanner and CT scanner to provide sequential PET and CT scans using a common imaging table.<sup>30,31</sup> These works introduced a new era in nuclear medicine imaging. These combinations permit the acquisition of emission and transmission data sequentially in a single study with the patient in an ideally fixed position. Thus, the two data sets can be acquired in a registered format by appropriate calibrations, permitting the acquisition of corresponding slices from the two modalities. The CT data can then be used to correct for tissue attenuation in the emission scans on a slice-by-slice basis. Since the CT data are acquired in a higher resolution matrix than the emission data, it is necessary to decrease the resolution of the CT data to match that of the emission data. In other words, the CT data are blurred to match the emission data for attenuation correction.

One additional topic must be addressed in order to ensure the accuracy of the attenuation correction. The output of the x-ray tube used in CT provides a spectrum of photon energies from 0 keV up to the maximum photon energy (kVp = peak energy in keV) setting used for the acquisition as shown in Fig. I.1.16. Because low-energy photons are preferentially absorbed in tissue, the beam spectrum shifts toward the higher energy end as it passes through more tissue, thereby changing its effective  $\mu$  and producing a variety of artifacts (beam-hardening effects) in images, and filtering of the beam to remove low-energy photons is required. The spectrum after filtering shown in Fig. I.1.16 has been “hardened” to reduce these effects. The resulting spectrum has an effective energy (mean) of approximately 70 keV in the example in Fig. I.1.16. Since attenuation effects vary with energy, it is necessary to convert the attenuation data acquired with CT to match the energy of the radionuclide used in the SPECT or PET acquisitions. For example in Fig. I.1.16, it is necessary to convert the attenuation data measured at an effective energy of 70–140 keV for <sup>99m</sup>Tc. This is typically accomplished by using a bilinear model<sup>32–34</sup> relating attenuation coefficients at the desired energy to CT numbers measured at the effective energy of the CT beam of x-rays as shown in Fig. I.1.17. For CT numbers < 0, the measured tissue is assumed to be a combination of air and water, and the attenuation coefficient at the desired energy (140 keV) can be calculated from the CT number by the equation.

$$\mu_{\text{tissue}, 140 \text{ keV}} = \frac{\text{CT\#} * (\mu_{\text{water}, 140 \text{ keV}} - \mu_{\text{air}, 140 \text{ keV}})}{1000}$$

This equation describes the first component of the bilinear curve in Fig. I.1.17. For CT numbers > 0, the conversion is more complicated due to the measured tissue being a



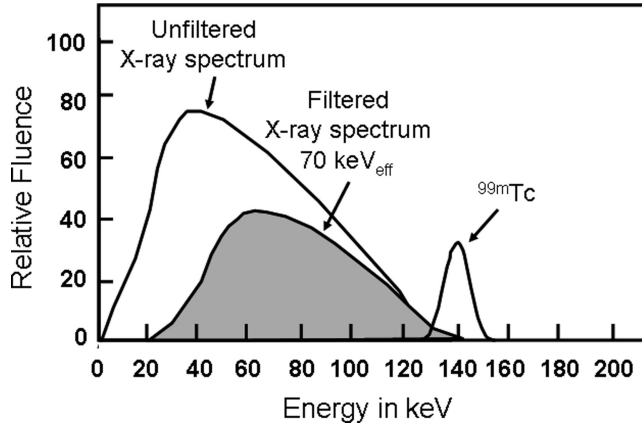
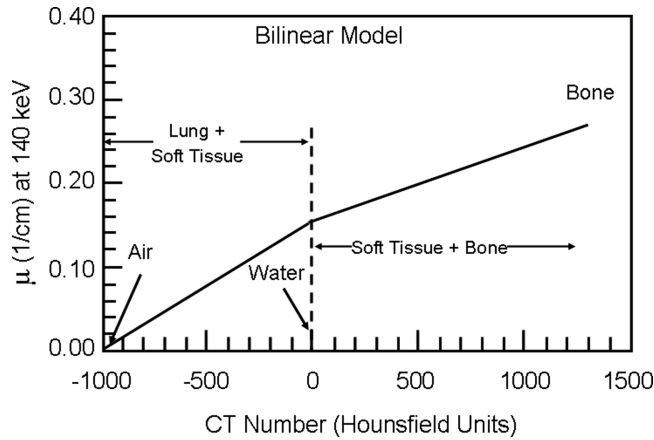


**Fig. I.1.16** Typical energy spectrum of x-rays from an x-ray tube. The shaded area shows the effects of filtration (beam hardening), which is used for CT scanning. These data can be used for attenuation correction of single photon emitters such as  $^{99m}\text{Tc}$  using the bilinear model shown in Fig. I.1.17 (Reprinted by permission of the Society of Nuclear Medicine from: James A. Patton and Timothy G. Turkington. SPECT/CT Physical Principles and Attenuation Correction. *J Nucl Med Technol* 2008 36(1):1–10. Fig. 7.)

**Fig. I.1.17** Bilinear model commonly used for converting measured CT numbers to attenuation coefficients for a specific radionuclide such as  $^{99m}\text{Tc}$  (Reprinted by permission of the Society of Nuclear Medicine from: James A. Patton and Timothy G. Turkington. SPECT/CT Physical Principles and Attenuation Correction. *J Nucl Med Technol* 2008 36(1):1–10. Fig. 8.)



combination of water and bone. In this case, the attenuation coefficient at the desired energy (140 keV) can be calculated from the CT number by the equation

$$\mu_{\text{tissue}, 140 \text{ keV}} = \mu_{\text{water}, 140 \text{ keV}} + \frac{\text{CT\#} * \mu_{\text{water}, \text{keVeff}} * (\mu_{\text{bone}, 140 \text{ keV}} - \mu_{\text{water}, 140 \text{ keV}})}{1000 * (\mu_{\text{bone}, \text{keVeff}} - \mu_{\text{water}, \text{keVeff}})}$$

This equation describes the second component of the bilinear curve in Fig. I.1.17. In practice, the various attenuation coefficients for specific photon energy used in the SPECT or PET acquisition and the effective photon energy used in the CT acquisition can be found in a stored look-up table in the reconstruction algorithm. The conversion can then be performed using two simple linear relationships relating the attenuation

coefficient at the desired energy and the measured CT numbers for specific measured tissues. From the attenuation coefficient data acquired with CT, correction factors can then be determined as shown in Fig. I.1.16, which can then be used to correct the SPECT or PET data (Fig. I.1.18) for attenuation, yielding the attenuation-corrected SPECT or PET images.<sup>35,36</sup>

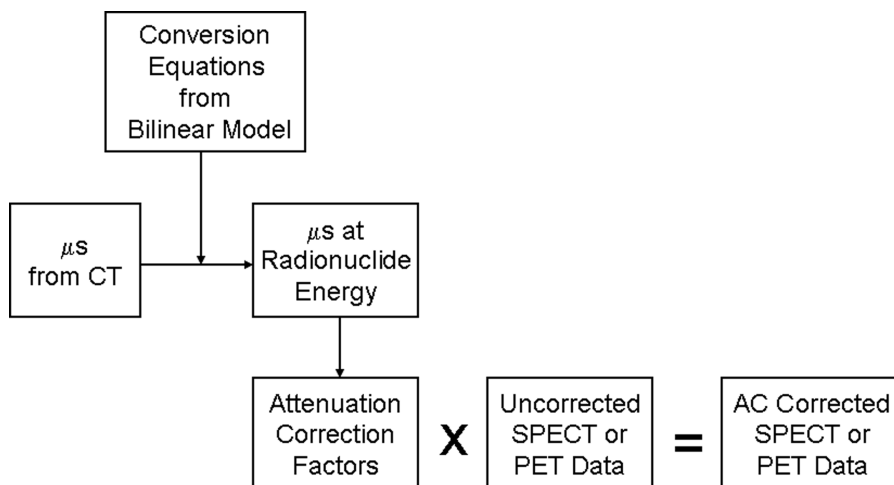


**Fig. I.1.18** Conversion equations from the bilinear model are used to convert attenuation coefficient values (ms) measured with CT to values corresponding to the energy of the radionuclide being imaged in order to determine factors for attenuation correction of SPECT or PET data

There are numerous advantages in the use of CT data for attenuation correction of emission data. First, the CT scan provides a very high photon flux which significantly reduces the statistical noise associated with the correction in comparison to other techniques (i.e., radionuclides used as transmission sources). Also, due to the fast acquisition speed of CT scanners, the total imaging time is significantly reduced by using this technology. Another advantage related to the high photon flux of CT scanners is that attenuation measurements can be made in the presence of radionuclide distributions with negligible contributions from photons emitted by the radionuclides (i.e., post-injection CT measurements can be performed). The use of CT also eliminates the need for additional hardware and transmission sources that often must be replaced on a routine basis. And, of course, the anatomical images acquired with CT can be fused with the emission images to provide functional anatomical maps for accurate localization of radiopharmaceutical uptake.

### ***Clinical SPECT/CT Systems***

Clinical SPECT/CT systems currently available from manufacturers typically have dual-head scintillation cameras positioned in front of the CT scanner and sharing a common imaging table. There are two approaches to clinical SPECT/CT applications. The first approach is the use of a low-output, slow-acquisition CT scanner, the Hawkeye<sup>®</sup> with

dual-head Infinia<sup>TM</sup> manufactured by General Electric Healthcare Systems. The CT scanner consists of a low-output x-ray tube (2.5 mA) and four linear arrays of detectors and can acquire four 5-mm anatomical slices in 13.6 s with a high contrast spatial resolution  $> 3$  lp/cm. The images acquired with this system are not of sufficient quality to be used for billable procedures, but are sufficient to be used for attenuation correction and anatomical correlation with emission scans. The slow scan speed is actually an advantage in regions where there is physiological motion since the CT image blurring from the motion is comparable to that of the emission scans resulting in a good match in fused images. Radiation dose from this system is typically  $< 5$  mGy (500 mrad) compared to values of 10–100  $\mu$ Gy (1–10 mrad) for applications using radioisotope transmission sources.

The second approach is to integrate commercially available CT scanners with dual-head scintillation cameras. The Symbia<sup>®</sup> with dual-head E-Cam manufactured by Siemens Medical Systems is available at present in one, two, and six slice versions with variable tube currents (20–345 mA), slice thicknesses of 0.6–10 mm, and rotational speeds of 0.6–1.5 s. The Precedence with dual-head Skylight manufactured by Philips Medical Systems is available in 16 and 64 slice versions with variable tube currents (20–500 mA), slice thicknesses of 0.6–12 mm, and rotational speeds as fast as 0.5 s. These systems exhibit high contrast spatial resolutions of 13–15 lp/cm with approximately 4–5 times the patient radiation dose of that from the Hawkeye<sup>®</sup> system. Since the CT scanners in the systems are commercially available diagnostic systems, the images produced are of sufficient quality to be used for billable procedures, in addition to the obvious attenuation correction and anatomical correlation applications. Radiation doses from these systems are on the order of 20 mGy (2 rads) when diagnostic quality images are produced. It should be noted that these systems can also be operated in a lower radiation dose mode by reducing the x-ray tube current. Although the images provided by this mode of operation typically are not of sufficient quality to be used for billable procedures, they are acceptable for attenuation correction and anatomical correlation applications.

### ***Clinical PET/CT Systems***

Clinical PET/CT systems are only available with diagnostic CT scanners, and systems are generally acquired with 4, 8, 16, or 64 slice capability providing images of sufficient diagnostic quality to be used for billable procedures. As with SPECT/CT systems, the CT scanners can be operated at reduced tube current if the scans are only to be used for attenuation correction.

### ***Contrast Agents***

Many diagnostic applications of CT scanning require the use of contrast agents administered either orally or intravenously to improve the visualization of soft tissue structures in the body. However, the use of a contrast CT scan for attenuation correction is a source of some concern. The introduction of a dense, high atomic number agent such as iodine increases the attenuation coefficients of the regions of tissue in which the contrast agent is located. This presence visually enhances the region in CT images by increasing the attenuation of the radiation beam in that region. However, when using the contrast CT scan for attenuation correction, the measured attenuation coefficients will be artificially increased potentially resulting in an artificial enhancement of the radionuclide distribution in the regions containing the contrast agent. In

other words, the potential exists for the creation of artifacts of increased radionuclide uptake in those regions. For this reason, caution is indicated in the use of contrast CT scans for attenuation correction, and it is advised that the uncorrected SPECT or PET scan be carefully reviewed to insure that no artifacts have been created in the corrected images.

### ***Beam-Hardening Artifacts***

It is not uncommon to see streak artifacts in CT scans in regions of the body containing dense bony structures. These artifacts are due to the preferential absorption of low-energy photons by the structures resulting in streaks of decreased photon flux in the final images. This phenomenon, known as beam hardening, is more severe in regions where metal objects such as surgical clips and prosthetic devices are present. In many instances, the presence of these artifacts will invalidate the use of the CT scan for attenuation correction in those regions.

### ***Physiological Motion***

The accurate registration of a SPECT or PET scan with a CT scan depends on careful calibrations of the sequential data acquisition processes and assumes that there is no patient movement during the acquisitions. However, the natural physiological motion of the lungs and heart poses potential problems. These problems exist due to the fact that CT acquisitions are fast, i.e., images of multiple slices are acquired in less than a second, and SPECT and PET acquisitions are slow, i.e., several minutes per view. The relatively fast motion of the heart results in the motion being smoothed out in both data sets so that a reasonable registration is usually obtained. However, the slower motion of the lungs often results in a misregistration at the base of the lungs that can cause difficulty in the accurate localization of lesions in this area. PET/CT systems are now available with respiratory gating capability so that both the CT and the PET scan of the chest can accurately be registered by eliminating the effects of lung motion.

### ***Radiation Dosimetry Considerations***

The replacement of conventional transmission sources with CT increases the concern regarding radiation dose to the patient. In the past, the radiation dose from transmission sources such as  $^{153}\text{Gd}$  used in SPECT and  $^{68}\text{Ge}$  used in PET was generally ignored due to the small values associated with their use in comparison to the dose from the radionuclides used in these studies. For example, the effective dose equivalent (EDE) for a PET transmission scan with  $^{68}\text{Ge}$  is on the order of 0.12 milli-Sieverts (mSv). However, when CT is used, the associated dose with this procedure is of such magnitude that it must be taken into consideration. The EDE for a diagnostic CT of the chest/abdomen/pelvis is on the order of 13 mSv assuming 140 kVp, 340 mA, 0.5 s rotation time, 5 mm slice, and 17.5 cm/s table feed. For comparison purposes, the EDE from a PET scan with 10 mCi of  $^{18}\text{F}$ FDG is 11 mSv<sup>37</sup> and from a SPECT scan with 25 mCi of  $^{99\text{m}}\text{Tc}$  labeled white cells is 18.5 mSv.<sup>37</sup> Thus, the addition of the diagnostic CT increases the dose by 118% and 70%, respectively, in these two examples. If the CT scan is only to be used for attenuation correction, the tube current (mA) can be reduced by a factor of 4 or more, reducing the EDE to no more than 3.3 mSv. The attenuation measurement with CT would then increase the total EDE by only 30% and 18%, respectively, in the two examples. Every patient's

study should be reviewed carefully prior to beginning the study in order that the CT acquisition parameters can be adjusted to achieve the desired data while minimizing radiation dose.

*Quality Assurance*

In addition to the routine quality assurance procedures that are routinely performed with CT scanners and scintillation cameras with SPECT capability, it is important to routinely verify the accuracy of the registration techniques that are used with these combined systems. Errors in registration will cause inaccuracies in attenuation correction procedures and improper correlations of anatomy and function. All manufacturers recommend the scanning of an image registration phantom, such as the one shown in Fig. I.1.19, with recommended weekly or monthly frequencies. The phantom shown in Fig. I.1.19 has six radioactivity-filled syringes that are positioned along the three imaging axes. The phantom is scanned sequentially with the CT scanner, and scintillation camera and errors are calculated between the measured center locations of the syringes. These measurements are then compared with the acceptable errors for the system, typically 3–5 mm, in order to verify that the registration accuracy is sufficient for clinical applications. It may be important to do these measurements with substantial weight on the table to mimic the clinical situation.

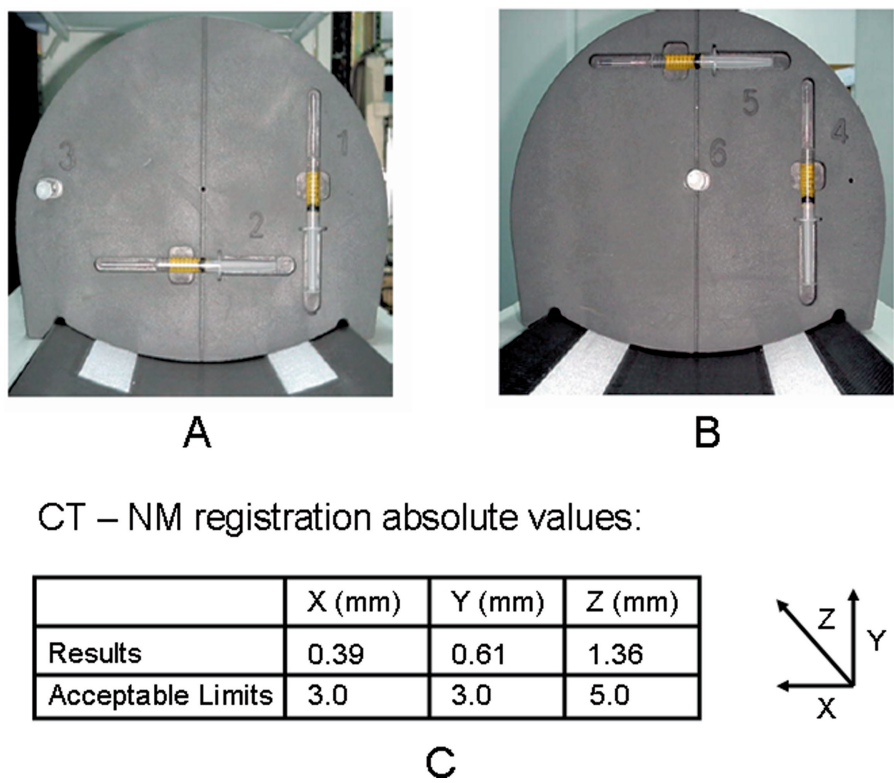


**Fig. I.1.19** (A–C) Phantom used for quality assurance of the registration of images acquired with CT and SPECT in an integrated system (Reprinted by permission of the Society of Nuclear Medicine from: James A. Patton and Timothy G. Turkington. SPECT/CT Physical Principles and Attenuation Correction. *J Nucl Med Technol* 2008 36(1):1–10. Fig. 15.)

Currently, the most common application of attenuation correction techniques in nuclear medicine is cardiac perfusion imaging.<sup>38</sup> The use of an accurate attenuation correction can provide valuable information in making the correct diagnostic interpretation. However, slight misalignments of the transmission and emission scans, often due to patient motion, can result in artifacts in the attenuation-corrected images. Because of this potential problem, manufacturers typically provide correction software to adjust the alignment of the two data sets. An example of currently available attenuation correction quality control (ACQC) software provided by General Electric Healthcare Systems is shown in Fig. I.1.20. In Fig. I.1.20B, CT images of the myocardium in the standard three orthogonal views format are shown with the perfusion images fused to this data set and presented as contours typically set at 30% of maximum counts. In these images, there is an obvious misalignment that results in attenuation-corrected images with artifacts of decreased perfusion as shown in Fig. I.1.20A. Under cursor control, the data sets can be re-aligned in the three views resulting in correct alignment as shown in Fig. I.1.20D. This results in the production of accurate attenuation-corrected perfusion images (Fig. I.1.20C). This is a valuable quality assurance technique that should be used regularly to validate registration prior to final image reconstruction and display in order to increase the level of confidence of the interpreting physician.<sup>39</sup>

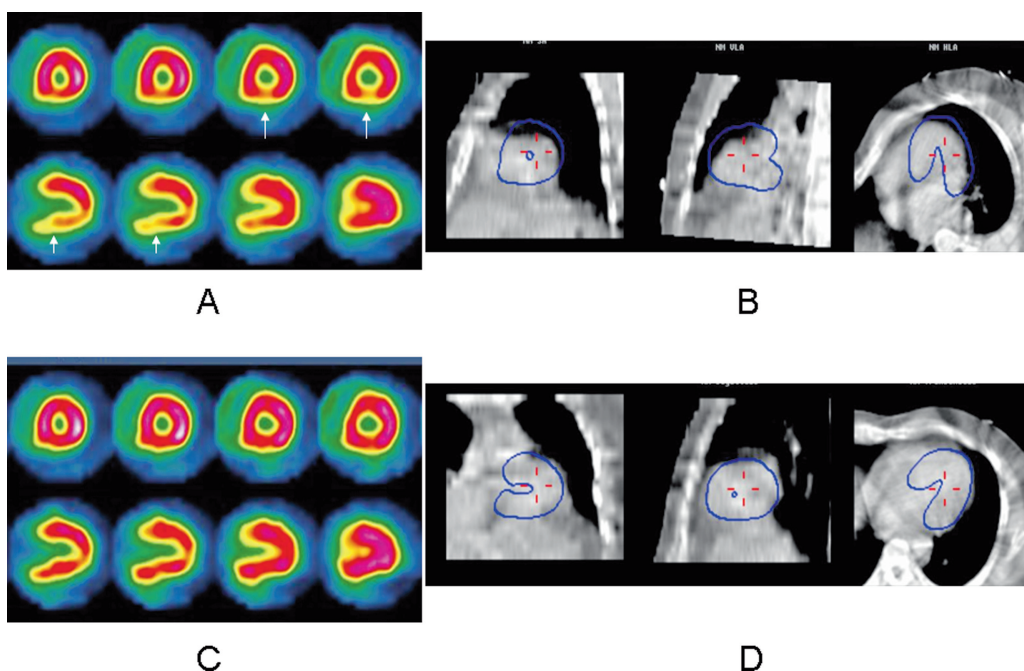


**Fig. I.1.20** Demonstration of the attenuation correction artifacts in a perfusion study (A) resulting from a misalignment of the CT and SPECT data sets (B) and the removal of these artifacts (C) after a re-alignment of the data sets (D) using registration quality assurance software (Reprinted by permission of the Society of Nuclear Medicine from: James A. Patton and Timothy G. Turkington. SPECT/CT Physical Principles and Attenuation Correction. *J Nucl Med Technol* 2008 36(1):1–10. Fig. 16.)

## Conclusions

The impact of the availability of hybrid imaging systems has been significant to diagnostic imaging. This impact is emphasized by the fact that during the past 2 years many scintillation cameras and most PET scanners have been purchased in combination with CT scanners in hybrid configurations. Clinicians now have the ability to image radiopharmaceutical distributions in registered format with anatomical images to accurately correlate function with anatomy and to improve image quality using the anatomical data for attenuation correction. This technology significantly improves the overall quality of the diagnostic information obtained and also provides data to improve therapeutic decisions thus enhancing patient care. The hybrid technology is now being extended to PET/MRI systems, and further advances are foreseen with this new capability.



## References

1. Anger HO, Rosenthal DJ. Scintillation camera and positron camera. In *Medical Radioisotope Scanning*. Vienna: International Atomic Energy Agency, 1959:59–75.
2. Kuhl DE, Edwards RQ. Image separation radioisotope scanning. *Radiology* 1963;80:653–662.
3. Kuhl DE, Edwards RQ. Cylindrical and section radioisotope scanning of the liver and brain. *Radiology* 1964;83:926–936.
4. Kuhl DE. A clinical radioisotope scanner for cylindrical and section scanning. In *Medical Radioisotope Scanning*, Vol. 1. Vienna: International Atomic Energy Agency, 1964:273–289.
5. Muehllehner G. A tomographic scintillation camera. *Phy Med Biol* 1971;16:87–96.
6. Keyes JW, Oleandea N, Heetderks WJ, Leonard PF, Rogers, WL. The humongotron: A scintillation camera transaxial tomography. *J Nucl Med* 1977;18:381–387.
7. Jaszcak RJ, Huard D, Murphy P, Burdine J. Radionuclide emission tomography with a scintillation camera. *J Nucl Med* 1976;17:551.
8. Galt JR, Germano G. Advances in instrumentation for cardiac SPECT. In DePuey EG, Berman DS, Garcia EV (eds): *Cardiac SPECT Imaging*. New York: Raven Press, 1995:91–102.
9. Garcia EV (ed). Imaging guidelines for nuclear cardiology procedures, part I. *J Nucl Cardiol* 1996;3:G3–45.
10. Shepp LA, Vardi Y. Maximum likelihood reconstruction for emission tomography. *IEEE Trans Med Imaging* 1982;MI-1:113–122.
11. Hudson HM, Larkin RS. Accelerated image reconstruction using ordered subsets of projection data. *J Nucl Med* 1994;13:601–609.
12. Muehllehner G, Buchin M, Dudek J. Performance parameters of a positron imaging camera. *IEEE Trans Nucl Sci* 1976;NS-23:528–537.
13. Patton JA. Instrumentation for coincidence imaging with multihead cameras. *Semin Nucl Med* 2000;30:239–254.
14. Robertson J, Marr R, Roseblum B. Thirty-two crystal positron transverse section detector. In Freedman G (ed): *Tomographic Imaging in Nuclear Medicine*. New York: Society of Nuclear Medicine, 1973:151–153.
15. Burnham C, Brownell G. A multi-crystal positron camera. *IEEE Trans Nucl Sci* 1972;19:201–205.
16. Brownell G, Burnham C. MGH positron camera. In Freedman G (ed): *Tomographic Imaging in Nuclear Medicine*. New York: Society of Nuclear Medicine, 1973:154–164.
17. Ter-Pogossian MM, Phelps ME, Hoffman EJ, Mullani N. A positron-emission transaxial tomography for nuclear imaging (PETT). *Radiology* 1975;114:89–98.
18. Phelps ME, Hoffman E, Mullani N, Ter-Pogossian MM. Application of annihilation coincidence detection to transaxial reconstruction tomography. *J Nucl Med* 1975;16:210–224.
19. Phelps ME, Hoffman E, Mullani N, Higgins CS, Ter-Pogossian MM. Design considerations for a positron emission transaxial tomography (PETT III). *IEEE Trans Nucl Sci* 1976;NS-23:516–522.
20. Hoffman E, Phelps ME, Mullani N, Higgins CS, Ter-Pogossian MM. Design and performance characteristics of a whole body transaxial tomography. *J Nucl Med* 1976;17:493–503.
21. Phelps ME, Hoffman E, Huang S, Kuhl D. ECAT: A new computerized tomographic imaging system for positron emitting radiopharmaceuticals. *J Nucl Med* 1978;19:635–647.
22. Hoffman E, Ricci A, van der Stee LMAM, Phelps ME. ECATIII – Basic design considerations. *IEEE Trans Nucl Sci* 1983;NS-30:729–733.
23. Hounsfield G, Ambrose J. Computerized transverse axial scanning (tomography). Part I: Description of system. Part II: Clinical applications. *Br J Radiol* 1973;46:1016–1047.
24. McCormack A. Reconstruction of densities from their projections, with applications to radiological physics. *Phys Med Biol* 1973;18:195–207.
25. X-Ray Computed Tomography. In Bushberg JT, Seibert JA, Leidholdt, Jr. EM, Boone JM (eds): *The Essential Physics of Medical Imaging, Second Edition*. Philadelphia: Lippincott Williams & Wilkins, 2002:327–369.
26. Bruyant PP. Analytic and iterative reconstruction algorithms in SPECT. *J Nucl Med* 2002;43:1343–1358.
27. Lang TF, Hasegawa BH, Liew SC, Brown JK, Blankespoor S, Reilly SM, Gingold EL, Cann CE. A prototype emission-transmission imaging system. *IEEE Nucl Sci Symp Conf Rec* 1991;3:1902–1906.
28. Lang TF, Hasegawa BH, Liew SC, Brown JK, Blankespoor CS, Reilly SM, Gingold EL, Cann CE. Description of a prototype emission-transmission computed tomography imaging system. *J Nucl Med* 1992;33:1881–1887.

29. Patton JA, Delbeke D, Sandler MP. Image fusion using an integrated, dual-head coincidence camera with X-ray tube-based attenuation maps. *J Nucl Med* 2000;41:1364–1368.
30. Townsend DW, Beyer T, Kinahan PE, Brun T, Roddy R, Nutt R, Byars LG. The SMART scanner: A combined PET/CT tomography for clinical oncology. *IEEE Nucl Sci Symp Conf Rec* 1998;2:170–1174, paper M5-1.
31. Beyer T, Townsend DW, Brun T, Kinahan PE, Charron M, Roddy R, Jerin J, Young J, Byars L, Nutt R. A combined PET/CT scanner for clinical oncology. *J Nucl Med* 2000;41:1369–1379.
32. Kinahan PE, Hasegawa BH, Beyer T. X-ray-based attenuation correction for positron emission tomography/computed tomography scanners. *Semin Nuc Med* 2003;33:166–179.
33. LaCroix KJ, Tsui BMW, Hasegawa BH, Brown JK. Investigation of the use of X-ray CT images for attenuation compensation in SPECT. *IEEE Trans Nucl Sci* 1994; NS-41:2793–2799.
34. Blankespoor SC, Xu X, Kalki CK, Brown JK, Tang HR, Cann CE, Hasegawa BH. Attenuation correction of SPECT using X-ray CT on an emission-transmission CT system: Myocardial perfusion assessment. *IEEE Trans Nucl Sci* 1996; NS-43:2263–2274.
35. Zaidi H, Hasegawa BH. Determination of the attenuation map in emission tomography. *J Nucl Med* 2003;44:291–315.
36. King MA, Glick SJ, Pretorius PH, Wells RG, Gifford HC, Narayanan MV, Farncombe T. Attenuation, scatter, and spatial resolution compensation in SPECT. In Wernick MN, Aarsvold JN (eds): *Emission Tomography: The Fundamentals of PET and SPECT*. London: Elsevier Academic Press, 2004:473–494.
37. Stabin, M, Stubbs JB, Toohey RE. *Radiation Dose Estimates for Radiopharmaceuticals*. Oak Ridge, TN: Radiation Internal Dose Information Center, ORNL, 1996.
38. Shaw LJ, Berman DS, Bax JJ, Brown KA, Cohen MC, Hendel RC, Mahmarian JJ, Williams KA, Ziffer JA. Computed tomographic imaging within nuclear cardiology, ASNC information statement – approved November 2004. *J Nucl Cardiol* 2005;12:131–142.
39. Tonge CM, Ellul G, Pandit M, Lawson RS, Shields RA, Arumugam P, Prescott MC. The value of registration correction in the attenuation correction of myocardial SPECT studies using low resolution computed tomography images. *Nucl Med Commun* 2006;27:843–852.

<http://www.springer.com/978-0-387-92819-7>

Hybrid PET/CT and SPECT/CT Imaging

A Teaching File

Delbeke, D.; Israel, O. (Eds.)

2010, XXX, 762 p. 300 illus. in color. With CD-ROM.,

Hardcover

ISBN: 978-0-387-92819-7